Mechanisms for the Interannual Variability of SST in the East Pacific Warm Pool

KRISTOPHER B. KARNAUSKAS

Lamont-Doherty Earth Observatory, Columbia University, Palisades, New York

ANTONIO J. BUSALACCHI

Earth System Science Interdisciplinary Center, University of Maryland, College Park, College Park, Maryland

(Manuscript received 5 February 2008, in final form 18 September 2008)

ABSTRACT

In comparison with the western and equatorial Pacific Ocean, relatively little is known about the east Pacific warm pool (EPWP). Observations indicate that the interannual variability of sea surface temperature (SST) in the EPWP is highly correlated (0.95) with the El Niño–Southern Oscillation (ENSO). In this paper, an ocean general circulation model (OGCM) of the tropical Pacific Ocean and various atmospheric and oceanic observations are used to diagnose the physical processes governing the interannual variability of SST in the EPWP. Atmospheric forcings for the OGCM are derived purely from satellite observations between 1988 and 2004.

Shortwave heating is identified as playing a dominant role in the interannual SST tendency of the EPWP. The high correlation between SST in the EPWP and eastern equatorial Pacific is therefore explained not by ocean processes, but by an atmospheric link. ENSO-driven equatorial SST anomalies modify the distribution of the overlying atmospheric vertical motions and therefore cloud cover and ultimately shortwave heating. During an El Niño event, for example, the ITCZ is equatorward displaced from its normal position over the EPWP, resulting in anomalously large shortwave heating over the EPWP. Analysis of poleward ocean heat transport and coastal Kelvin waves confirms that oceanic processes are not sufficient to explain the interannual variability of the EPWP.

1. Introduction

In recent decades, a great deal of research has been invested in the coupled ocean–atmosphere system of the western and equatorial Pacific Ocean. The Tropical Ocean and Global Atmosphere (TOGA) program greatly advanced our understanding of the western tropical Pacific Ocean (McPhaden et al. 1998). Motivation for interest in the western Pacific Ocean is its critical role in atmospheric convection and the overlying Walker circulation. During the TOGA decade, the Coupled Ocean–Atmosphere Response Experiment (TOGA COARE) aimed to provide an understanding of the role of the warm pool regions of the tropics in the mean and transient state of the tropical ocean–atmosphere system (Webster and Lukas 1992). In comparison, relatively little is known about the warm pool in the eastern tropical Pacific Ocean. Only in the last decade has attention begun to shift to the east, including the Pan American Climate Studies program (PACS), the Eastern Pacific Investigation of Climate (EPIC), the Climate Variability and Predictability (CLIVAR) North American Monsoon Experiment (NAME), the Global Energy and Water Cycle Experiment (GEWEX), and the upcoming CLIVAR Inter-Americas Study of Climate Processes (IASCLIP).

In terms of sea surface temperature (SST), there are three major large-scale features of the tropical Pacific Ocean (Fig. 1). Dominating the western tropical Pacific is the massive west Pacific warm pool (WPWP). In the eastern tropical Pacific, the SST field is dominated by a meridional gradient between the equatorial Pacific cold tongue (CT) and the east Pacific warm pool (EPWP). The CT is the site of large interannual variations of SST due to the El Niño–Southern Oscillation (ENSO). The thermocline in the tropical Pacific slopes upward from west to east. That is, the WPWP is associated with a very

Corresponding author address: Dr. Kristopher B. Karnauskas, Lamont-Doherty Earth Observatory, Columbia University, 301E Oceanography Bldg., 61 Route 9W, Palisades, NY 10964.
E-mail: krisk@ldeo.columbia.edu

DOI: 10.1175/2008JCLI2467.1

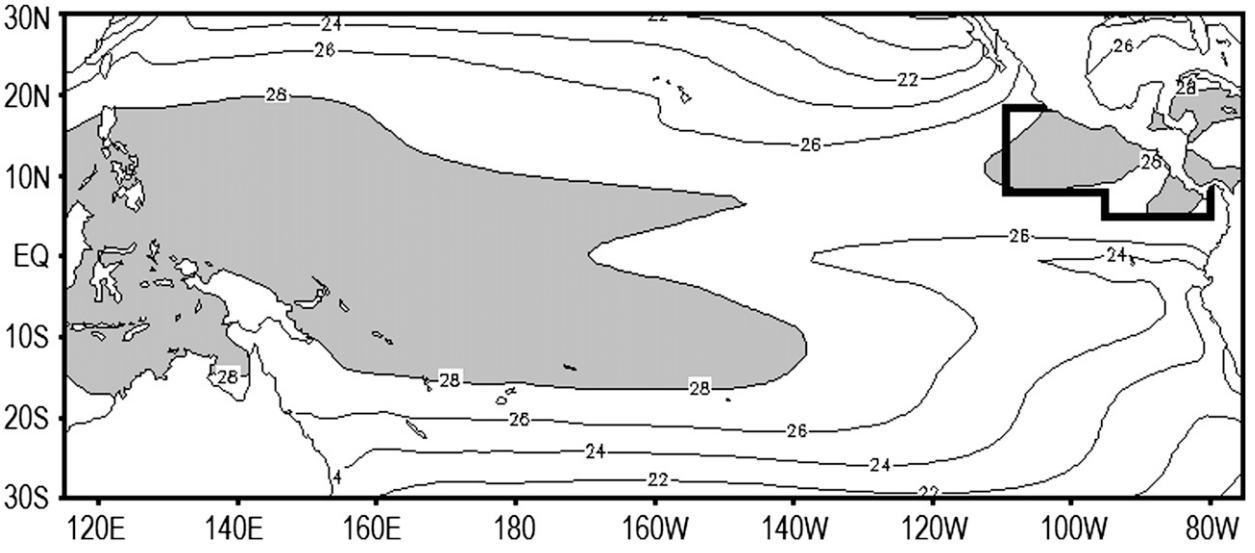

FIG. 1. Map of annual mean SST in the tropical Pacific (°C) for the period 1982–2006 (Reynolds OI v.2). The box represents the region used for constructing an index of area-averaged SST anomaly in the EPWP.

deep thermocline (~150 m), while the CT and EPWP are situated within a relatively shallow background thermocline (meters to tens of meters in the CT, and ~75 m in the EPWP). As one would expect based on the above description of the mean subsurface thermal structure of the tropical Pacific Ocean, the mean balance and temporal variations of SST in the WPWP are essentially a one-dimensional radiative equilibrium. In contrast, one expects dynamical processes to regulate the depth of the thermocline and mixing across the base of the mixed layer to regulate SST in the equatorial Pacific.

Although the size of the EPWP does not compare to the WPWP, the magnitude of the SST within it, and potential climatic consequences, do compare. The EPWP is a region of intense air–sea interaction on intraseasonal and seasonal time scales (Maloney and Kiehl 2002; Maloney and Esbensen 2003, 2005; Xie et al. 2005). On interannual time scales, even if SST in the EPWP has smaller variability than that in, say, the CT, it is operating at a higher mean temperature where even small changes thereof have significant effects on tropical convection (Zhang 1993; Wang and Enfield 2001).

There are five major reasons why an improved understanding of the interannual variability of SST in the EPWP is important:

1) SST in the EPWP plays an important role in the interannual variability of rainfall over Central America. In terms of a first-order spatial scale, the intertropical convergence zone (ITCZ) over the EPWP is part of a tropics-wide belt of heavy precipitation, and therefore rainfall over Central America can be considered within that context (Karnauskas and Busalacchi 2009). Collier et al. (2004) identified the EPWP/Central America region as one of two major rainfall biases in boreal summer in the National Center for Atmospheric Research (NCAR) Community Climate Model, version 3 (CCM3; Kiehl et al. 1996). The other is located over the central Indian Ocean. The magnitude of the bias is nearly 10 mm day^{-1} relative to satellite measurements by the Tropical Rainfall Measuring Mission (TRMM; Kummerow et al. 2000).
2) The EPWP is the main development region (MDR) for eastern North Pacific tropical cyclones (Sadler 1964). Since SST is an important boundary condition to transient tropical mesoscale phenomena such as tropical cyclones, an improved understanding of the interannual variability of SST in the EPWP would contribute to the understanding of eastern North Pacific tropical cyclones.
3) The interannual variability of SST in the EPWP is linked to that of near-surface regional ocean biology from plankton to mammals. Numerous studies have identified the EPWP as a ''hotspot'' for ocean biology. Fiedler (2002) focused on the seasonal cycle of SST in the EPWP and implications for phytoplankton, whales, and dolphins. Much of the seminal work of K. Wyrtki was done with tuna fisheries in mind (e.g., Wyrtki 1964a,b). Given that processes governing SST also have the potential to regulate the availability of nutrients from below and sunlight from above, understanding the interannual variability

of SST in the EPWP helps with understanding its impact on the marine food web.

4) The EPWP could play an important role in the evolution of ENSO, including regional and global teleconnections associated with ENSO. The EPWP is situated within ~10° latitude of the eastern equatorial Pacific Ocean, where ENSO-related SST anomalies are most prominently manifested. Sun (2000) suggested that poleward heat transport by the ocean is considerable following El Niño events. What role does the EPWP play in the evolution of ENSO events?
5) The EPWP can be considered a part of a broader tropical warm pool with global atmospheric effects. In this paper, the EPWP is examined as an independent warm pool located exclusively within the Pacific Ocean. However, several recent studies by investigators at the National Oceanic and Atmospheric Administration/Atlantic Oceanographic and Meteorological Laboratory (NOAA/AOML) consider the EPWP a part of a much broader "Western Hemisphere warm pool" (WHWP) that also includes the Caribbean Sea, Gulf of Mexico, and in some cases, the tropical Atlantic Ocean (Wang and Enfield 2001, 2003; Lee et al. 2005; Enfield and Lee 2005; Wang et al. 2006; Enfield et al. 2006; Lee et al. 2007). The present work is complementary to the recent work by the AOML investigators by examining in detail one of the components of the WHWP.

The WHWP was introduced in Wang and Enfield (2001). The rationale is that, taken together, the WHWP is a major tropical heating center interfacing with the atmosphere, much like the Indo-Pacific warm pool, with important influences and teleconnections around the globe. Wang and Enfield (2001, 2003) described the first-order balance and the annual cycle in the WHWP region, concluding that SST in the northeastern tropical Pacific is controlled mainly by the anomalous Pacific mixed layer associated with ENSO, although this was not accompanied by analysis. Lee et al. (2005) and Enfield and Lee (2005) returned to the annual cycle in the WHWP, finding again that the annual cycle in the Pacific part of the WHWP is dominated by net surface flux.

Wang et al. (2006) investigated how the non-Pacific part of the WHWP influences summer rainfall and Atlantic hurricanes. Enfield et al. (2006) focused on how ENSO events force the non-Pacific part of the WHWP to be anomalously large and/or warm. Finally, Lee et al. (2007) used models to reexamine the annual cycle of the WHWP. According to Lee et al. (2007), the WHWP "cannot be considered as a monolithic whole with a single set of dominating processes that explain its behavior." Clearly it is time for a study aimed specifically at the interannual variability of the Pacific part of the WHWP—that is, the EPWP. This paper represents the first of such an attempt.

The organization of the remainder of the paper is as follows. The datasets, ocean model, and experiments are described in the following section. The results of the ocean model experiments and supporting analyses are discussed in section 3. Finally, a summary is provided in section 4.

2. Methodology

a. Model description

The ocean model used in the present study is the Gent and Cane (1989) reduced gravity, primitive equation, sigma-coordinate (potential density) OGCM of the tropical oceans. There are three primary mechanisms for ocean turbulent mixing: entrainment–detrainment, shear flow instability, and convection in the thermocline. The version of the Gent–Cane OGCM used in the present study includes the hybrid vertical mixing scheme of Chen et al. (1994), which combines the classic mixed layer physics of Kraus and Turner (1967) with the Price et al. (1986) dynamic instability model to account for all three mechanisms for ocean mixing, and is thought to be more realistic than a constant-depth mixed layer or one with idealized physics. This OGCM setup has been shown to faithfully reproduce the mean state, annual cycle, and interannual variability in the tropical Pacific Ocean including the EPWP region (Chen et al. 1994; Kessler et al. 1998; Karnauskas 2007).

Our model setup also includes the Seager et al. (1995) atmospheric mixed layer (AML) model, which was coupled to the Gent–Cane OGCM by Murtugudde et al. (1996). The Seager et al. (1995) AML simulates the atmospheric advection of air temperature and humidity, after which heat fluxes are computed. Such a coupling allows a realistic representation of the feedbacks between SST and surface heat fluxes, but should not be confused with a fully coupled ocean–atmosphere GCM in which winds respond to SST, cloud cover responds to winds, etc.; the AML cannot change the prescribed dynamical wind stress or shortwave forcing.

The horizontal resolution of the OGCM in this study is uniform 1/3° zonal and meridional, and a reduced-order Shapiro filter of the order of 8 is applied to velocity and tracer fields once every 4 time steps, which increases computational stability by reducing grid-scale noise without affecting the physical structure of the fields. There are 20 layers in the vertical: a variable-depth mixed layer plus 19 subsurface layers. The model time

step is 30 min. The meridional boundaries of the model grid are 30°N–10°S, along which a sponge layer is used at the meridional open boundaries (see Chen et al. 1994). Zonal boundaries are represented by the approximate coastlines of Asia, Indonesia, Australia in the western Pacific (Indonesian throughflow is closed off), and the Americas in the eastern Pacific.

b. Model experiments

Following a 60-yr spinup period initialized with the climatology of Levitus and Boyer (1994), each integration spans 1988–2004, saving weekly averages. In addition to a control experiment, two experiments were performed to disentangle the roles of momentum versus heat flux forcing on the mixed layer heat budget in the EPWP. In this very simple experimental setup, one type of forcing was held to climatology while the others were interannually varying. The Control experiment included full interannual forcing. Experiment – (Clim–Solar) is the same as Control except that wind stress (shortwave) forcing was held to climatology. In this manner, differences between the Control and other experiments can be interpreted as the effect of the interannual forcing on the ocean, plus nonlinear effects.

c. Model forcing

Interannual wind stress forcing was derived from a wind stress dataset merging Special Sensor Microwave Imager (SSM/I) ocean surface winds and SeaWinds wind vectors. Both instruments have a nominal spatial resolution of 25 km. The merged wind stress dataset includes SSM/I using the variational analysis of Atlas et al. (1996) from 1988 to 1999 (version 10) and Quick Scatterometer (QuikSCAT) from 1999 to 2004, with a smooth conversion from SSM/I to QuikSCAT between July and September 1999. The QuikSCAT dataset was produced using the optimal interpolation method of Bourassa et al. (1999). The SSM/I–QuikSCAT wind stress data were regridded to a 1° by 1° horizontal grid with weekly temporal resolution. Interannual surface downward shortwave radiation forcing was derived from a product developed in conjunction with the Global Energy and Water Cycle Experiment (GEWEX) Surface Radiation Budget (SRB) project. The SRB product combines satellite observations of top-of-atmosphere fluxes with a radiative transfer model to infer the downward flux of shortwave radiation at the surface of the earth (Pinker and Laszlo 1992). This set of atmospheric forcing applied to the model described above produces a mean tropical Pacific climate, including SST, the mixed layer depth, and the seasonal heat budget in the EPWP region that validates well against observations (Karnauskas 2007).

d. Supporting datasets

To complement the ocean model experiments, several observation-based datasets are analyzed including SST from the NOAA/Optimal Interpolation version 2 (Reynolds et al. 2002), subsurface fields from the Simple Ocean Data Analysis (SODA; Carton et al. 2000), sea level from the Ocean Topography Experiment (TOPEX) altimeter (Fu et al. 1994), atmospheric fields such as humidity and vertical motion from the NCEP–NCAR global reanalysis (Kalnay et al. 1996), and outgoing longwave radiation (OLR) from the NOAA interpolated OLR dataset (Liebmann and Smith 1996).

3. Results

a. Simulated and observed SST

The objective of this section is to characterize the interannual variability of SST in the EPWP, and to make an assessment of the model fidelity in simulating interannual variability. We define an index of area-averaged SST anomaly that roughly corresponds to the annual mean 28°C isotherm. The index region is bounded to the west at 110°W, to the east at 80°W and the coast of Mexico–Central America, to the north at 18°N and the coast of Mexico–Central America, and to the south at 8°N west of 95°W and 5°N east of 95°W (Fig. 1). Shown in Fig. 2 (top panel) is the observed time evolution of SST anomaly in the EPWP and Niño-3 region (5°S–5°N, 150°–90°W) as derived from satellite observations. The interannual variability of SST in the EPWP and Niño-3 is clearly related (correlation 0.79). When a 13-month centered running mean is applied to both time series and Niño-3 leads by 2 months, the correlation is 0.95. There are three large ENSO events in the period shown (1982/83, 1987, and 1997/98), as manifested in Niño-3 SSTA. In each of those three cases, the SST anomaly in the EPWP corresponded very closely to that of the equatorial Pacific, if not lagging by a month or so. The early–mid-1990s and the 2000s were relatively absent of notable ENSO events, yet the SST anomaly time series shown in Fig. 2 still show many similarities during those inactive periods.

The cross correlation of the unsmoothed indices is shown in Fig. 3 (left panel). The maximum correlation is found when the EPWP lags Niño-3 by 1 ($r_t = 0.76$) and 2 ($r_t = 0.75$) months. Also shown in Fig. 3 are the autocorrelations of the indices themselves; Niño-3 decorrelates by 6–7 months, while the Niño-3–EPWP cross correlation remains higher than e^{-1} until 9 months. The EPWP index itself decorrelates faster than does Niño-3 in the first few months, but does not decay beyond e^{-1}

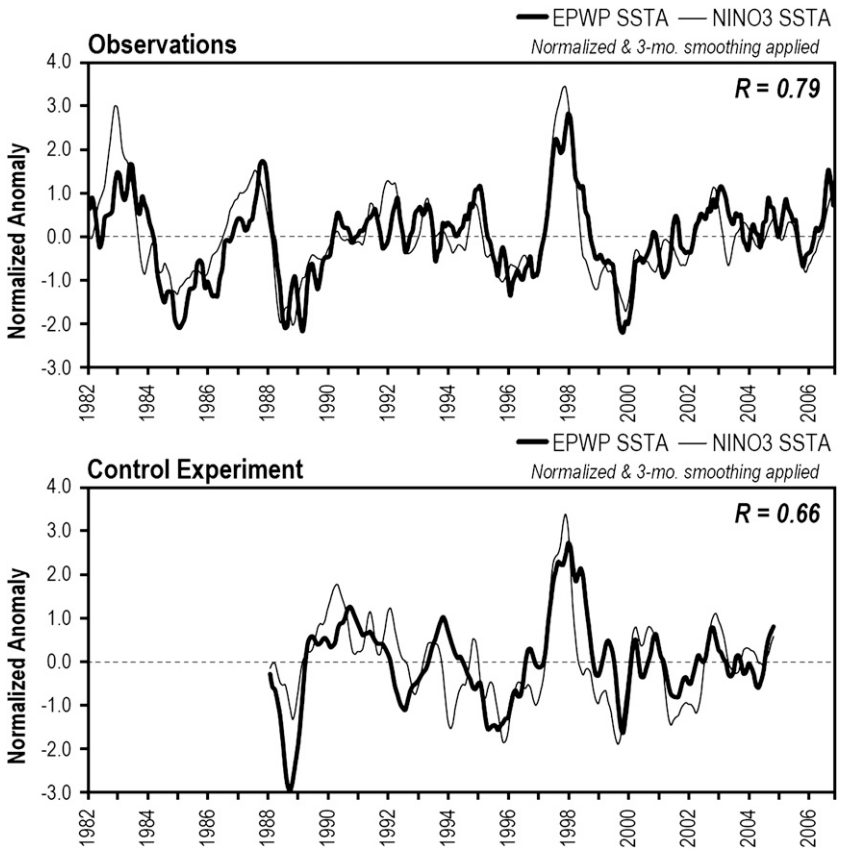

FIG. 2. (top) Observed (Reynolds OI v.2) monthly mean SST anomaly in the EPWP (thick black line) and the Niño-3 region (thin black line). (bottom) Simulated (Control experiment) monthly mean SST anomaly in the EPWP (thick black line) and Niño-3 (thin black line). All time series normalized and smoothed with a 3-month centered moving mean.

until 7 months, similar to Niño-3. Furthermore, there is a full 4-month period where the EPWP remains positively correlated with Niño-3 but Niño-3 itself has become anticorrelated (lag months 10–13, inclusive). This is evident in the right panel of Fig. 3, which indicates that the EPWP is more highly correlated with the Niño-3 index than the Niño-3 index is with itself for a full 16-month period beginning 4 months following a peak Niño-3 anomaly. With the understanding that the Niño-3 variance tends to peak in December, this period would tend to begin with the calendar month of April. This delayed retention of SST anomaly by the EPWP has important implications for the Central American hydroclimate (Karnauskas and Busalacchi 2009).

Shown in the bottom panel of Fig. 2 is the representation of SST in the EPWP and Niño-3 region as in the top panel, but for the ocean model Control simulation. Once again, there is a high correspondence between ENSO and the EPWP (correlation 0.66). The observed-to-modeled correlations are 0.72 (Niño-3) and 0.64 (Niño-3). The following sections are dedicated to understanding, from a mechanistic point of view, what controls the interannual variability of SST in the EPWP.

b. Interannual heat budget

The high correlation and lag between EPWP and Niño-3 SSTA suggests that the interannual variability of the EPWP is driven by ENSO. Therefore, the present discussion of mechanisms for interannual variability of EPWP SST is necessarily focused on the mechanisms for ENSO influencing the EPWP. If ENSO forces the EPWP, what is the method by which the ENSO signal is communicated to the EPWP? It is not clear whether the line of communication between the equator (ENSO) and the EPWP would be provided by ocean dynamics operating between the equator and the EPWP, such as equatorially forced waves propagating through the EPWP region, ENSO's modulation of the broader eastern equatorial thermocline (i.e., the canonical ENSO pattern) being broad enough to physically encompass the EPWP, poleward ocean heat transport, or through local coupling to the atmosphere. To provide an impression of

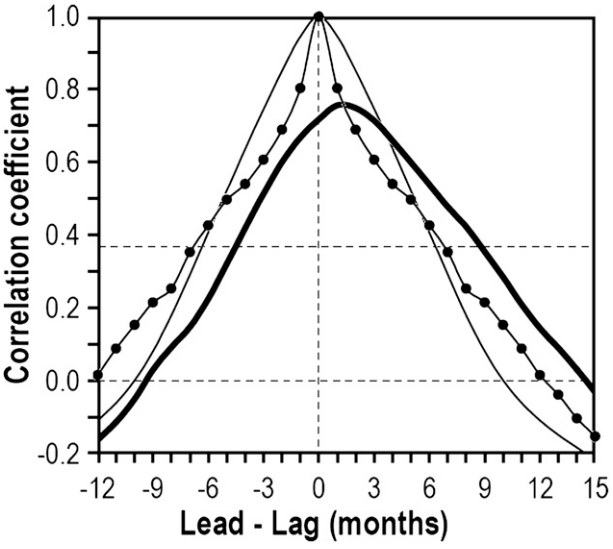

FIG. 3. Observed (Reynolds OI v.2) autocorrelation functions of the monthly unsmoothed Niño-3 (thin line) and EPWP (thin line with dots) SSTA indices, and cross correlation between the monthly unsmoothed Niño-3 and EPWP SSTA indices (heavy line) from the period 1982–2006. Positive values on the x axis are for the EPWP lagging Niño-3. Dashed lines mark zero months, zero correlation, and correlation = 0.367 (e^{-1}; the decorrelation time scale).

what processes are dominant, we turn to the model mixed layer ocean heat budget.

To simplify the portrayal of the mixed layer heat budget terms, advective flux terms (i.e., zonal heat flux, meridional heat flux, and entrainment–mixing) have been combined to form the "advective sum," and surface heat flux terms (i.e., shortwave radiation, longwave radiation, and latent and sensible heat flux) were combined to form the "surface sum." Thus, the surface sum includes both radiative and turbulent heat fluxes, which occur at the air–sea interface. The result of these calculations for the Control forced ocean model experiment, as well as the temperature tendency $\partial T/\partial t$, is presented in Fig. 4 (top panel). Our model results overwhelmingly suggest that the primary process by which surface ocean temperatures in the EPWP change is through surface heat fluxes, not advective fluxes (including entrainment–mixing). The correlation coefficient between the surface sum and $\partial T/\partial t$ time series is 0.88. The advective sum (anomaly) is in fact often of the opposite sign as $\partial T/\partial t$, meaning that the surface heat fluxes are driving the SST anomaly, while the advective fluxes may at times act to damp them. Discrepancies between $\partial T/\partial t$ and the surface sum are largely due to the advective sum.

Of the terms grouped into the surface sum, the surface shortwave radiation has by far the largest amplitude and is the only one that displays correspondence with the $\partial T/\partial t$ time series. Shown in Fig. 4 (bottom panel) is the evolution of the surface shortwave radiation Q_{SW} and $\partial T/\partial t$ indices for the EPWP over the Control experiment. The correlation between the surface sum and the surface shortwave radiation time series is 0.70, and the correlation between the surface shortwave radiation and

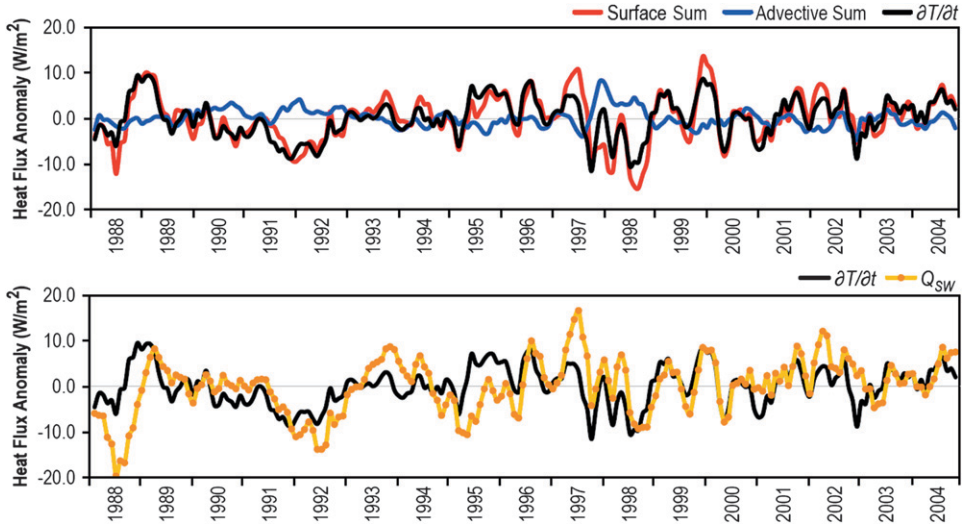

FIG. 4. (top) The time series of the sum of the surface heat fluxes ("surface sum," W m^{-2}, red line; shortwave, longwave, latent, and sensible), the sum of the advective heat fluxes ("advective sum," W m^{-2}, blue line; zonal heat flux, meridional heat flux, and entrainment–mixing), and $\partial T/\partial t$ (W m^{-2}, black line) for the EPWP. (bottom) As in the (top), but for $\partial T/\partial t$ (black line) and the surface shortwave radiation heat flux term ("Q_{SW}," W m^{-2}, orange line).

$\partial T/\partial t$ time series is 0.51. Of the dominant surface heat flux terms, shortwave radiation is the primary form of surface heat flux responsible for the evolution of the SST anomaly in the EPWP.

The remaining surface heat flux terms (longwave and turbulent flux terms) tend to be of opposite sign as $\partial T/\partial t$ and Q_{SW} and therefore slightly offset the surface shortwave anomaly, with the exception that latent heat flux plays a role in the mixed layer heat budget on slower time scales. The ocean–atmosphere latent heat flux (Q_{LH}) depends primarily on two factors: wind speed (W) and the moisture gradient at the air–sea interface (Δq). The Q_{LH} increases with both W and Δq. The magnitude of Δq depends on two factors: atmospheric specific humidity (q_a) and SST. Both Δq and thus Q_{LH} decrease with increasing q_a. By the Clausius–Clapeyron relation, the (saturation) specific humidity at the sea surface (q_s) increases with increasing SST, thus Δq increases with increasing q_s, and Q_{LH} increases with increasing SST. On the mean, Q_{LH} transfers energy from the ocean to the atmosphere everywhere over the global oceans. Only in very unusual cases is the transfer of energy via Q_{LH} from the atmosphere to the ocean. Ocean–atmosphere Q_{LH} is especially strong in the tropics, including the EPWP. In the equatorial Pacific cold tongue, Q_{LH} is a relative minimum. According to TAO estimates, the annual mean ocean–atmosphere Q_{LH} over the EPWP is roughly 100 W m^{-2}.

On short time scales, Q_{LH} acts as a negative feedback to SSTA. However, as evident in Fig. 5, on interannual and longer time scales, Q_{LH} contributes directly to SST variability in the EPWP. The Q_{LH} in Fig. 5 is shown in terms of its heat flux contribution to the ocean mixed layer heat budget, thus positive anomalies indicate a positive atmosphere–ocean Q_{LH} anomaly (physically interpreted as a reduced ocean–atmosphere Q_{LH} anomaly). The fact that the Q_{LH} and $\partial T/\partial t$ time series tend to have the same sign indicates that the low-frequency Q_{LH} is not forced by the local SST (otherwise it would be anticorrelated as if trying to damp SST anomalies). Rather, the low-frequency Q_{LH} is forcing a response in $\partial T/\partial t$ and Q_{LH} variability must be due to variations in W and/or q_a.

As previously noted, the EPWP lies directly beneath the ITCZ in the eastern tropical Pacific. This is because the ITCZ tends to situate itself directly over the warmest SSTs in the tropics, as they force large-scale ascent, convection, and provide a large supply of water vapor to the atmosphere. On the mean, the ITCZ is actually a region of minimum W and maximum q_a (Fig. 6), which is ideal for a minimum of ocean–atmosphere Q_{LH}. Low-frequency variations in the position of the ITCZ, along with its minimum W or maximum q_a, could thus strongly modulate the Q_{LH} and force a response in EPWP SST.

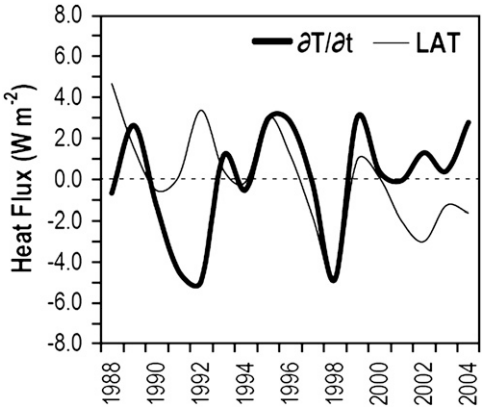

FIG. 5. Smoothed time series of annual mean $\partial T/\partial t$ anomaly (W m^{-2}, thick black line) and atmosphere–ocean Q_{LH} anomaly (W m^{-2}, thin black line) for the EPWP.

From the perspective of the mixed layer heat budget, it has been determined that the primary process governing the interannual variability of SST in the EPWP is surface shortwave radiation (Fig. 4). However, as shown in section 3a, the time series of SST anomaly in the EPWP and Niño-3 are a close match. The linkage must therefore be that ENSO influences surface shortwave radiation over the EPWP. During an El Niño event, for example, SST in the east-central equatorial Pacific becomes anomalously warm, which forces upward vertical motions and deep convection in the atmosphere (Zhang 1993), and compensating subsidence over the off-equatorial regions. Shown in Fig. 7a is a vertical cross section of annual mean omega (dp/dt) along 100°W from 20°S to 20°N averaged over the NCEP–NCAR reanalysis period (1948–2003). On the annual mean, the general distribution of vertical motions is characterized by strong ascent (i.e., the ITCZ) centered over 7.5°N, with broad descent everywhere south of 5°N, and some weak descent immediately north of the ITCZ. This depiction is qualitatively representative for the longitude range between 130° and 85°W. The strong ascent is situated 5°–10°N of the equator because the warmest SSTs lie north of the equatorial cold tongue, and thus the thermal equator at 100°W is effectively at 7.5°N. It is thus no surprise that the EPWP is also a region of high precipitation. However, using November 1997 as an example (Fig. 7b), El Niño events result in strong ascent anomalies over the geographical equator, as well as strong compensating descent anomalies over a band of latitudes roughly 5°–10°N, which corresponds with the location of the EPWP. Thus, during an El Niño event, there would tend to be less clouds and precipitation over the EPWP and a greater

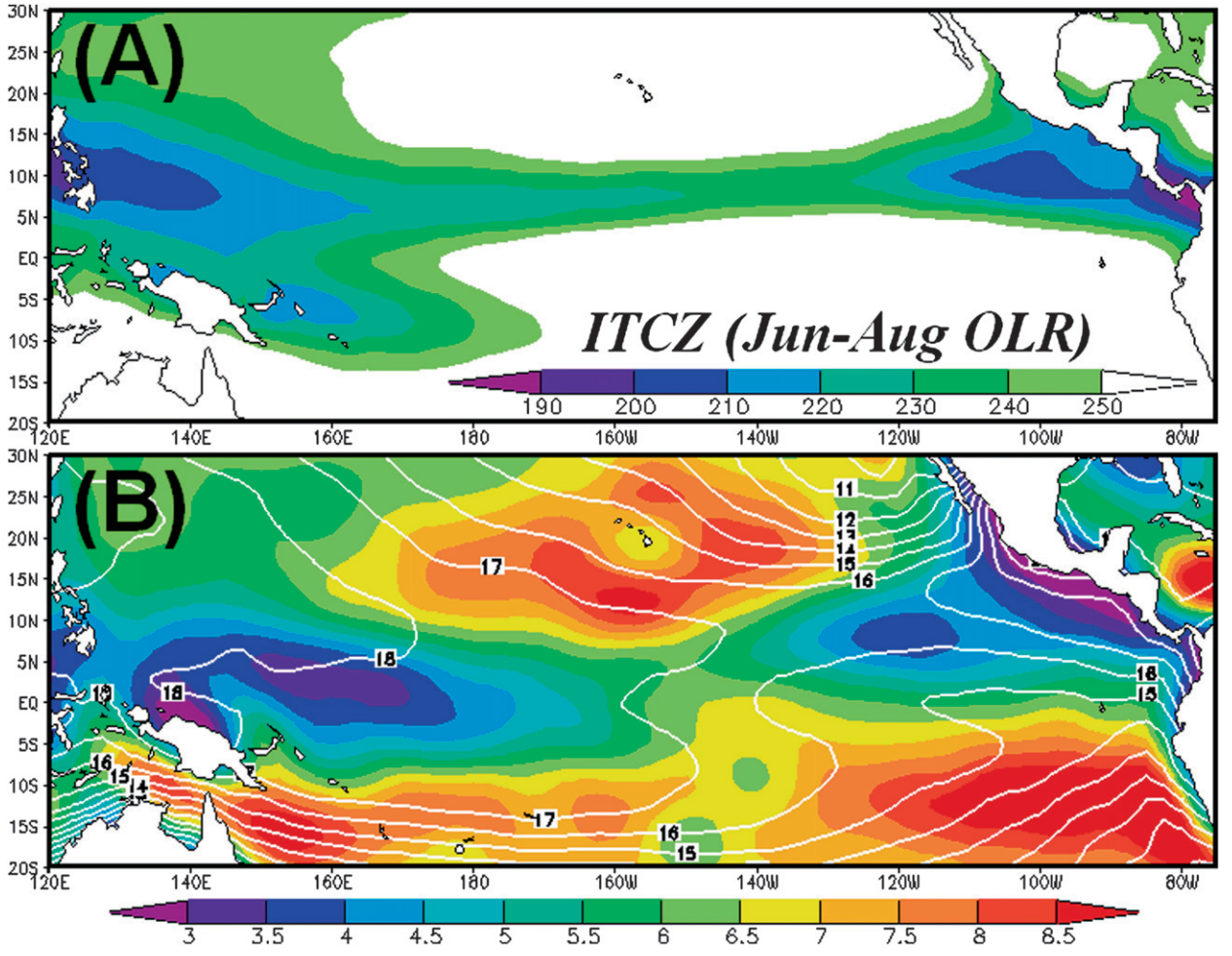

FIG. 6. (a) Boreal summertime (June–August climatological mean) position of the ITCZ in terms of OLR (W m^{-2}). (b) The 1000-hPa wind speed (m s^{-1}; shaded), and 1000-hPa specific humidity (g kg^{-1}; contoured). OLR from NOAA/interpolated OLR (AVHRR); W and q_a from the NCEP–NCAR reanalysis.

abundance of surface shortwave radiation available to heat the ocean surface. To establish that this is a statistically robust tropospheric response to ENSO, including the signal over the EPWP, Fig. 8 presents the correlation between the October–December mean omega anomaly and the Niño-3 index (correlations significant at the 95% confidence level shown). Negative correlations over the equatorial region (physically interpreted as ascent during the warm ENSO phase) exceed −0.6, and positive correlations over the EPWP (physically interpreted as descent during warm ENSO phase) exceed +0.6 over the 56 yr of the NCEP–NCAR reanalysis. These are, in fact, the only statistically significant features in the cross section.

To translate this response of the general circulation of the atmosphere into the heat flux forcing to the surface ocean, shown in Fig. 9 (left panels) is the regression of surface shortwave radiation anomalies onto the index of SST anomaly in the EPWP. Since the SSTA in the EPWP and Niño-3 regions are very similar, this can also be approximately interpreted as the regression onto a Niño-3 time series. In the regression using either simulated or observed SST, there is reduced shortwave radiation along the equator extending eastward approximately to the Galápagos Islands, and enhanced shortwave radiation to the north of the equator as well as over the EPWP. Such a configuration would be favorable for heating the ocean surface at the EPWP. Also shown in Fig. 9 (right panels) is the regression of SRB surface downward shortwave radiation anomalies onto $\partial T/\partial t$ in the EPWP. These plots indicate how much shortwave radiation is typically associated with a standard deviation of $\partial T/\partial t$. The values indicated by the regressions (6–9 W m^{-2}) are well within the range of variability of the surface shortwave radiation (13–17 W m^{-2} in the vicinity of the EPWP).

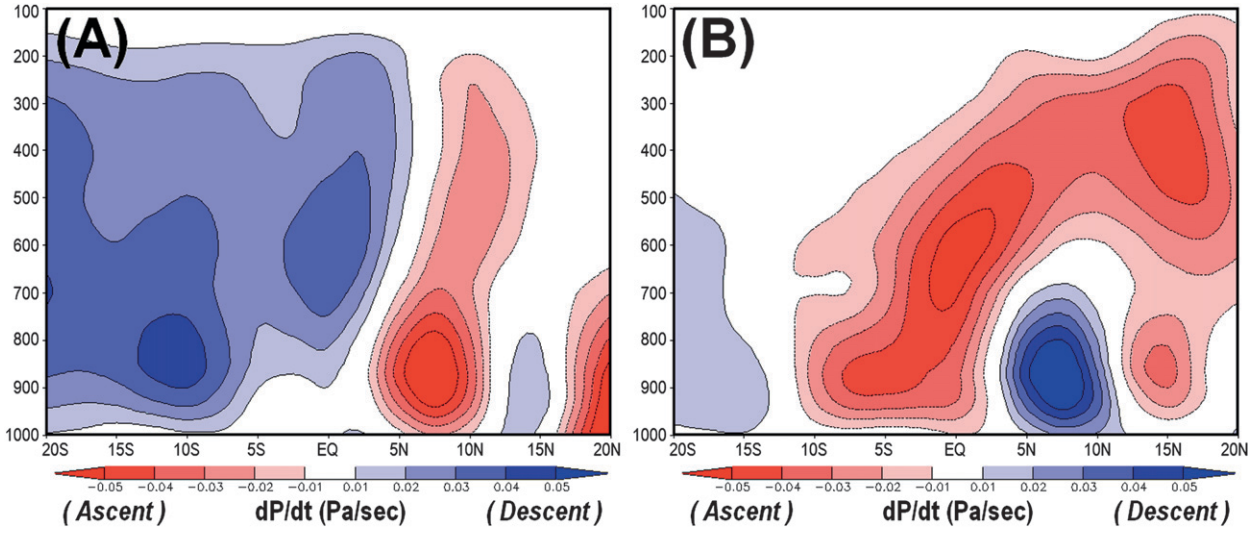

FIG. 7. Vertical cross section of annual mean (1948–2003) omega (dp/dt; Pa s^{-1}) along (a) 100°W and (b) the anomaly during November 1997 from the NCEP–NCAR reanalysis.

c. *The role of poleward ocean heat transport*

The weakness of the advective sum in Fig. 5 implies little connection between ocean transport and SST in the EPWP. Figure 10 provides a general picture of where there is high and low amplitude of sea level variability (SLA). In the TOPEX observations and the Control experiment, there is high SLA variability along the equator, which is primarily due to ENSO variability. There is also high SLA variability near the coast in the

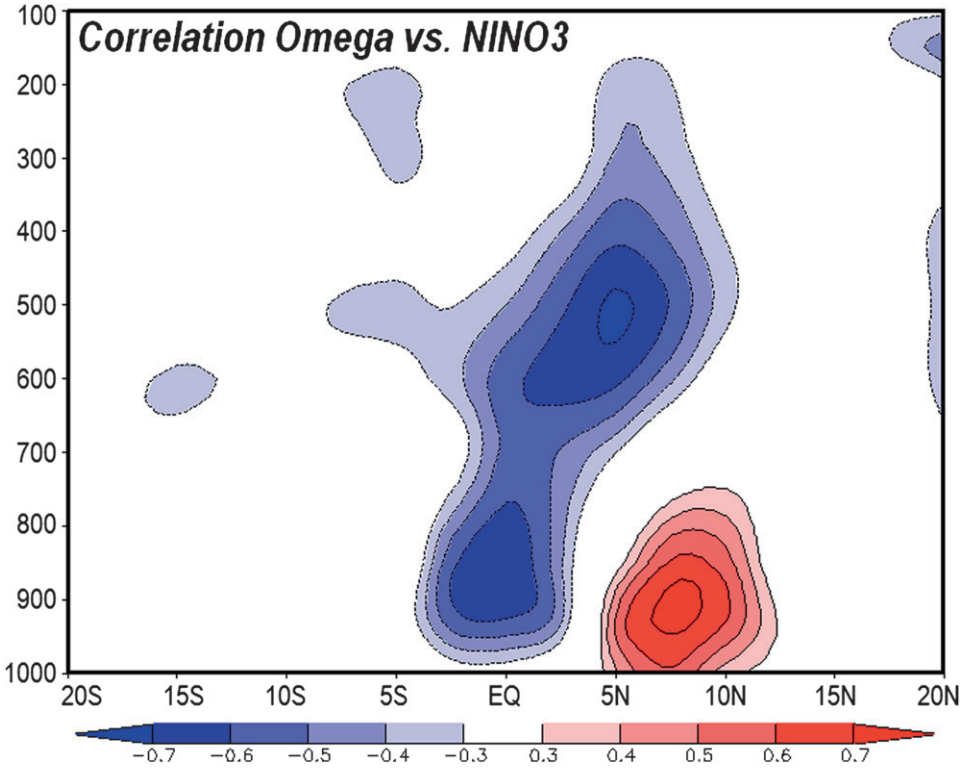

FIG. 8. Vertical cross section of the correlation between October–December mean omega anomaly and the Niño-3 index along 100°W from the NCEP–NCAR reanalysis (Kalnay et al. 1996) over the full reanalysis period (1948–2003).

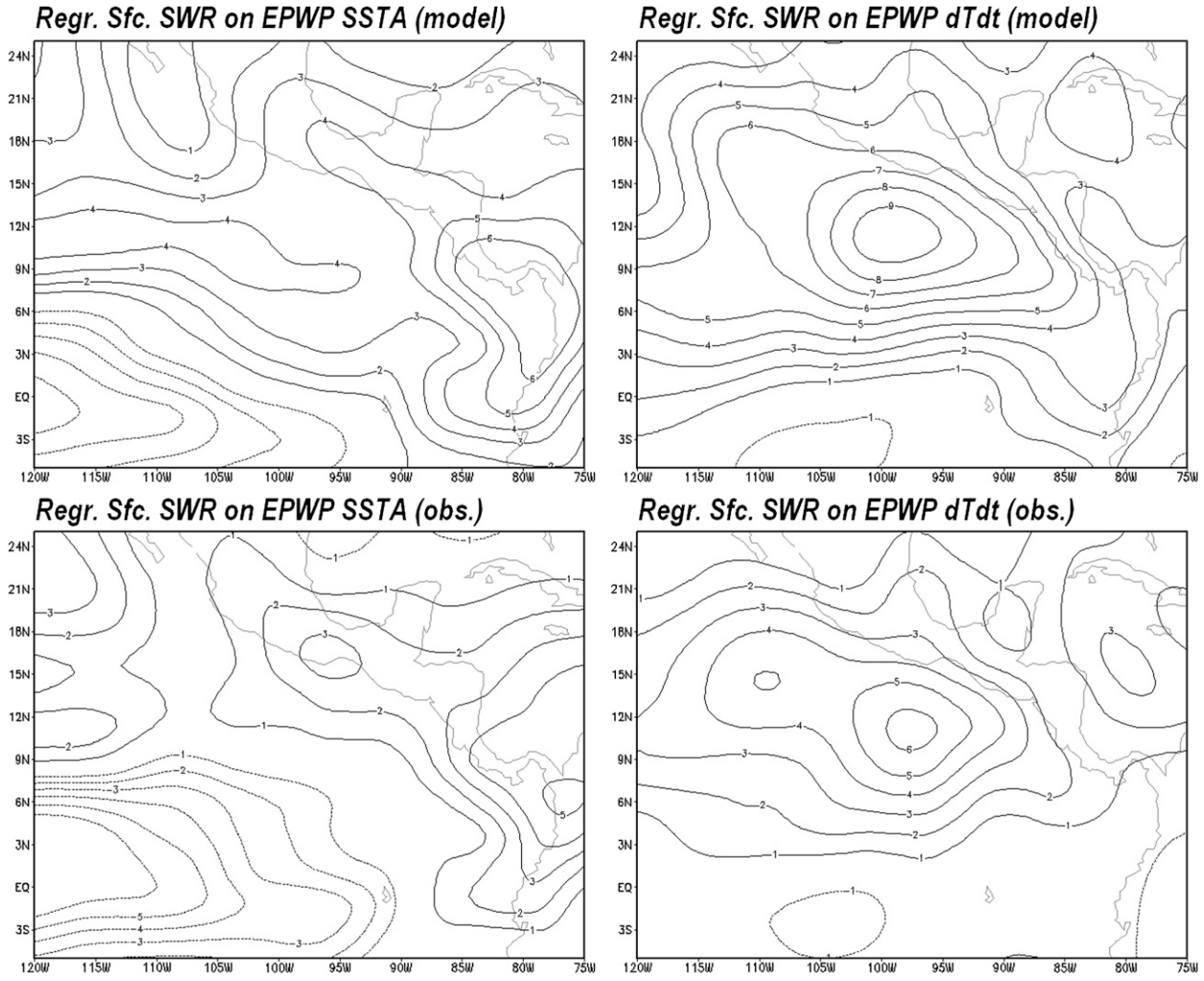

FIG. 9. Regression of SRB surface downward shortwave radiation anomaly (W m^{-2}, contour interval 1 W m^{-2}) onto (top) simulated and (bottom) observed indices of (left) the EPWP SST anomaly and (right) the time rate of change of the EPWP SST anomaly ($\partial T/\partial t$).

EPWP; coastally trapped Kelvin waves are a prominent feature of the northeastern tropical Pacific Ocean. However, also in both TOPEX observations and the Control experiment, there is a local minimum of SLA variability along 5°N in the TOPEX plot and 3°N in the Control experiment plot (i.e., the local minimum lies between the equator and the EPWP). The apparent separation between the equator and the EPWP region is stronger in the TOPEX observations than in the Control experiment, which may be due to model deficiencies, differing temporal periods over which the standard deviations were calculated, or altimeter deficiencies near the coast.

A subsurface examination of the 1997/98 El Niño and 1999–2000 La Niña events in the SODA reanalysis (Carton et al. 2000) is shown in Fig. 11. During the El Niño event, the equatorial SST is anomalously warm because the equatorial thermocline is ~100 m deeper than its climatological depth of ~40 m. From the SSTA time series discussed in section 3a, SSTA in the EPWP closely follows that of the Niño-3 region. Though the subsurface temperature anomaly in the EPWP is up to negative 4°C during the 1997/98 El Niño event, the thermocline in the EPWP is very close to its climatological depth. In the case of the 1999–2000 La Niña event (Fig. 11b), the equatorial SSTA is negative, which would be the logical result of the thermocline displaced upward from its climatological value of ~40 m to only ~5 m beneath the surface. However, in the heart of the EPWP (10°N), the thermocline is very near climatology, and there is evidence of even slightly positive temperature anomalies at depth, rather than strongly negative

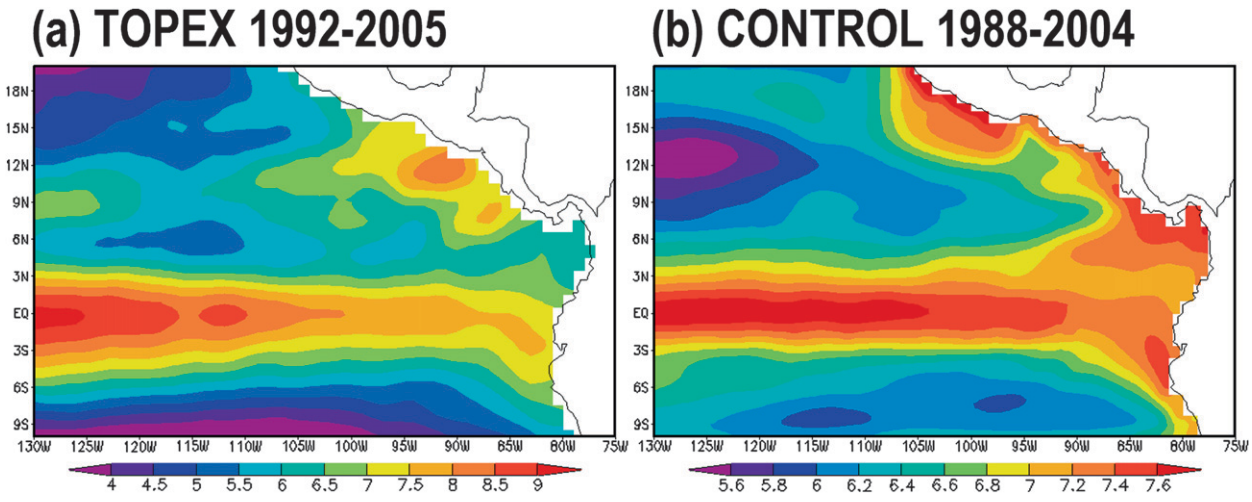

FIG. 10. Weekly standard deviation of SLA (cm) in the eastern tropical Pacific Ocean from (a) the TOPEX satellite altimetry for the period 1992–2005 and (b) the Control experiment for the period 1988–2004.

like the equator. Earlier cases were also analyzed in a similar fashion from the SODA reanalysis (1972/73, 1982/83, and 1986/87), and yielded very similar results as those discussed here. Progressing forward in time (i.e., January, February, March, etc.) from the case shown in Fig. 11a indicates that the positive temperature anomaly spreads poleward in both directions as a negative temperature anomaly begins to develop in its place. To the north, however, there is a strong horizontal density gradient separating the equatorial region from the EPWP (Fig. 11d). In addition, there is a strong vertical density gradient beneath the EPWP. Such strong horizontal and vertical density gradients effectively serve to surround the EPWP with a barrier of stratification to mixing with neighboring regions. A nearly identical structure as that shown in Fig. 11d can be found in TAO observations of potential density along 95°W (not shown). Since mixing and transport across isopycnals requires much greater energy than mixing and transport along isopycnals, the northward-propagating temperature anomaly is confined to within or below the pycnocline.

By April 1998 (Fig. 11c), the difficulty with which the northward-propagating temperature anomaly encounters to penetrate the density gradients surrounding the EPWP is evident; the majority of the positive temperature anomaly is still equatorward of 8°N (the southern latitudinal boundary of the EPWP defined in section 3a) from the surface to a depth of ~40 m. Clearly the preference is for propagation along the pycnocline, thus not greatly impacting the mixed layer heat budget of the EPWP. Figures 10–11 provide observational and experimental evidence of a disconnect in ocean dynamical processes between the equator and the EPWP, which is consistent with the notion that ENSO does not drive the interannual variability of SST in the EPWP through direct ocean dynamics and transport.

d. The role of coastal Kelvin waves

The final task in this section is to address the role of coastally trapped Kelvin waves (KWs) in the interannual variability of SST in the EPWP. Coastal KWs are an important feature of the circulation in the tropical Pacific Ocean, particularly the northeastern tropical Pacific (Kessler 2006) and thus the EPWP. As coastal KWs in this region can be equatorially forced, they could also provide an ocean connection between the equatorial Pacific and the EPWP, and thus a method of communication of the ENSO signal to the EPWP. The task is thus to determine the extent to which coastal KWs generate SST anomalies in the EPWP.

Shown in Fig. 12a is a ''boundary Hovmoeller'' of SSTA for the Control ocean model experiment. Time increases along the positive y axis, and the x axis represents distance, following the coast, from the equator and 20°N. For convenience, latitude is also marked on the x axis. Recall that the EPWP is generally within the latitude band from 5° to 15°N. Clearly evident in Fig. 12a are significant variations in coastal SSTA near the equator (out to about 6°N), and between 8° and 15°N. Between 6° and 8°N, there is a subtle break in the northward-propagating coastal signal. The SST anomalies near 15°N are associated with the Tehuantepec gap winds (Karnauskas et al. 2008). As Fig. 12a is for the Control experiment, this includes the contribution from interannual wind stress and surface shortwave radiation. Thus, from this depiction, it cannot be objectively determined what parts of, or how much of, the coastal SST

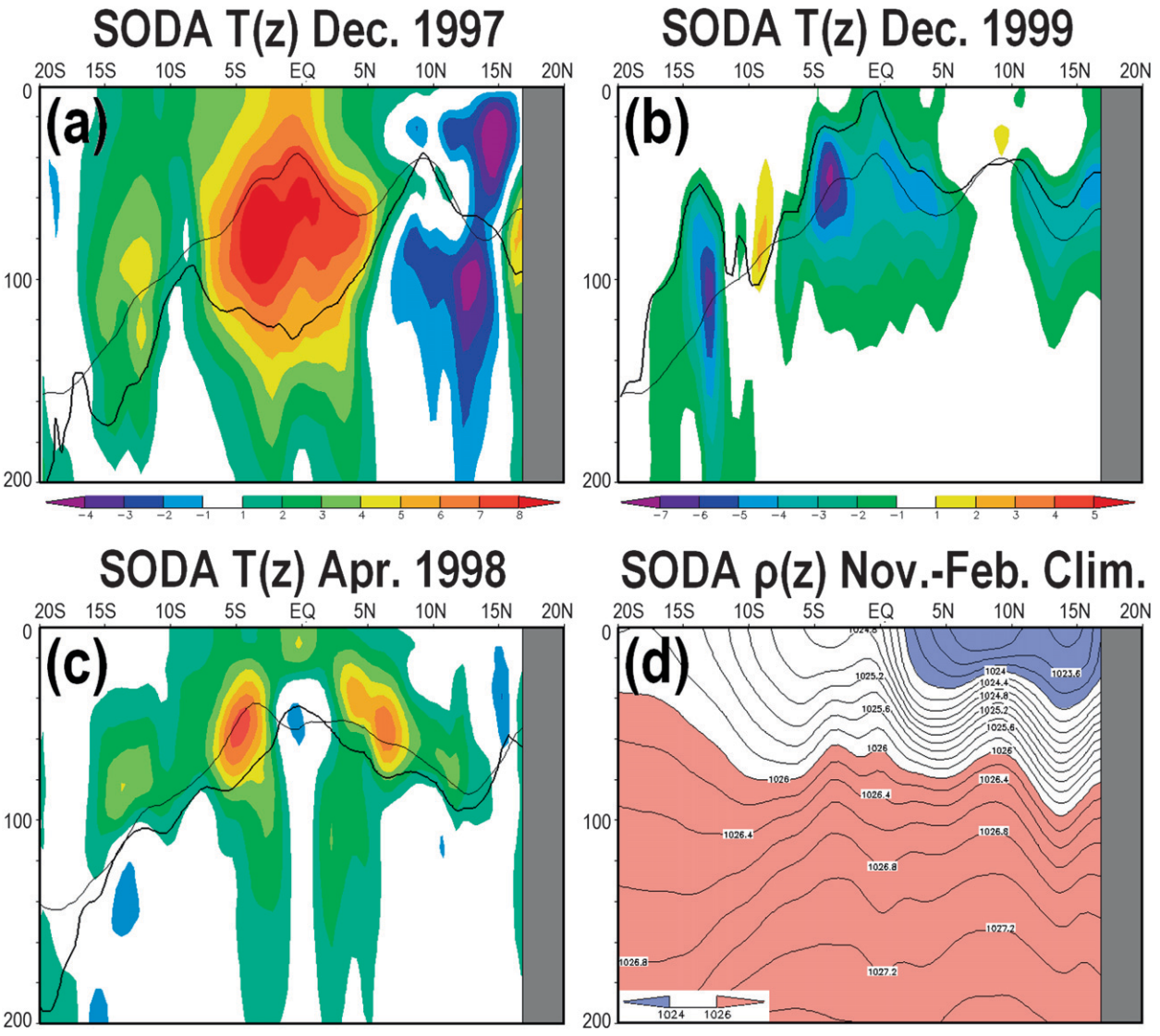

FIG. 11. (a) The vertical cross section of ocean temperature anomaly in the upper 200 m along 100°W from 20°S to 20°N (shaded, °C), the depth of the 20°C isotherm (heavy black line, m), and the depth of the climatological 20°C isotherm for that month (thin black line, m) during December 1997. (b) As in (a), but for December 1999. (c) As in (a), but for April 1998. (d) November–February climatological mean ocean density (kg m^{-3}) along the same section. All variables are computed from the SODA reanalysis (Carton et al. 2000). Gray shading indicates no data (the Pacific coast of Mexico).

anomalies are actually due to coastal KWs versus other processes. Shown in Fig. 12b is the same boundary Hovmoeller of SSTA, but for the Clim–winds ocean model experiment. In this experiment, there cannot be equatorially forced coastal KWs, as shortwave radiation alone cannot initiate KWs. As a consistency check, it is noted that the SSTA variations in the Gulf of Tehuantepec are absent from Fig. 12b. However, significant interannual SST variations a*re* present near the equator and in the latitude band encompassing the EPWP. Although it may seem surprising that there could be a signal near the equator without the interannual wind stress forcing, this is actually possible for two reasons: 1) as expected, the magnitude is smaller than that in the Control experiment (i.e., Fig. 12a), and 2) the shortwave regressions (Fig. 9, left panels) show that the positive surface shortwave radiation anomaly pattern does extend along the coast as far south as the equator. Within the latitude band of the EPWP, the SST variations in the Clim–winds experiment are nearly as large as those in the Control experiment. To confirm that these SST variations are in fact related to variations in shortwave radiation, shown in Fig. 12c is the corresponding boundary Hovmoeller diagram for SSTA in

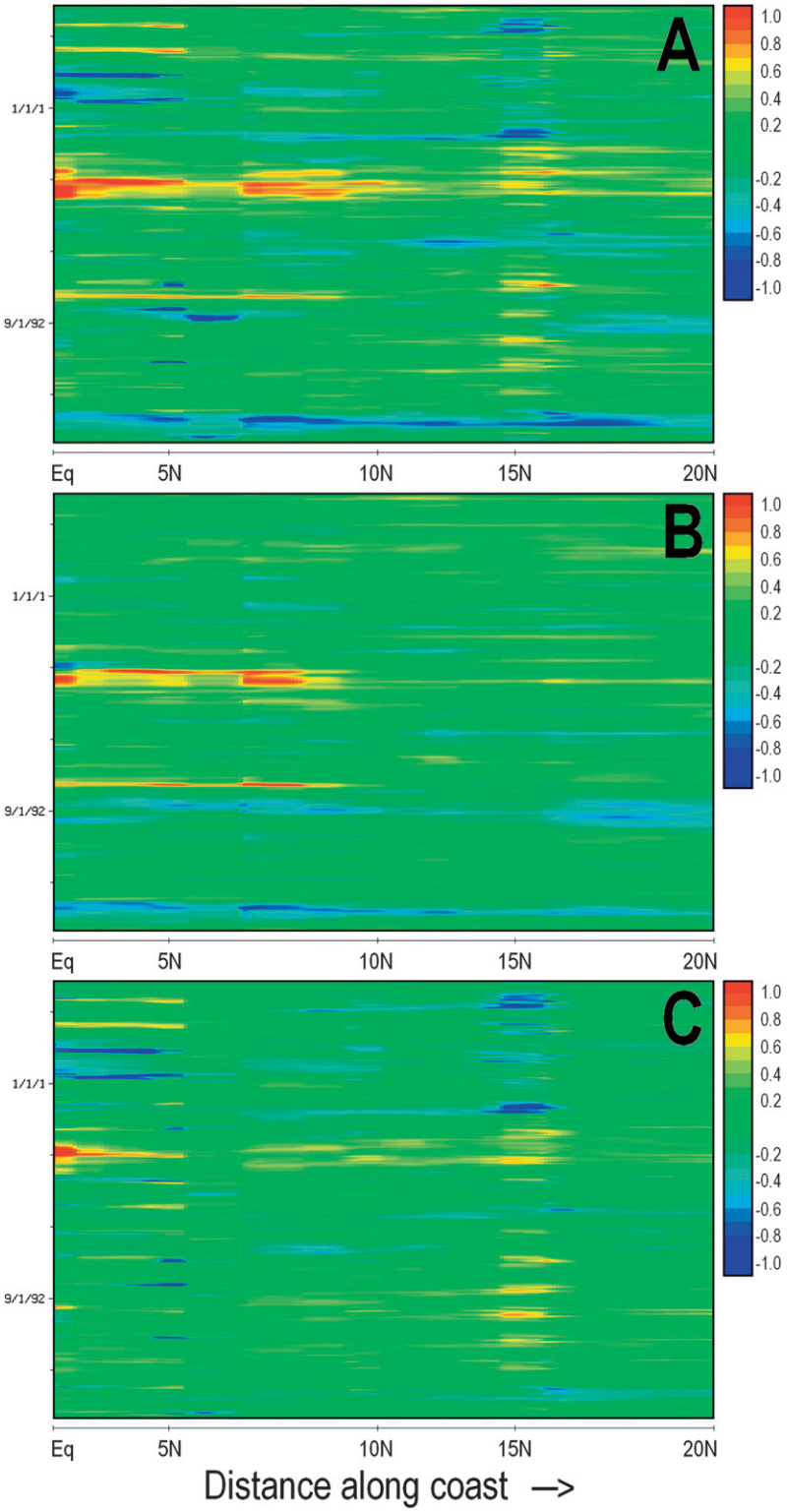

FIG. 12. Boundary Hovmoeller diagrams of SSTA (°C) along the Pacific coast of Central America and Mexico from the equator to 20°N in the (a) Control experiment, (b) Clim–winds experiment, and (c) Clim–solar experiment. Time increases along the positive *y* axis from January 1988 to December 2004. The color legend shown in the lower right applies to (a)–(c).

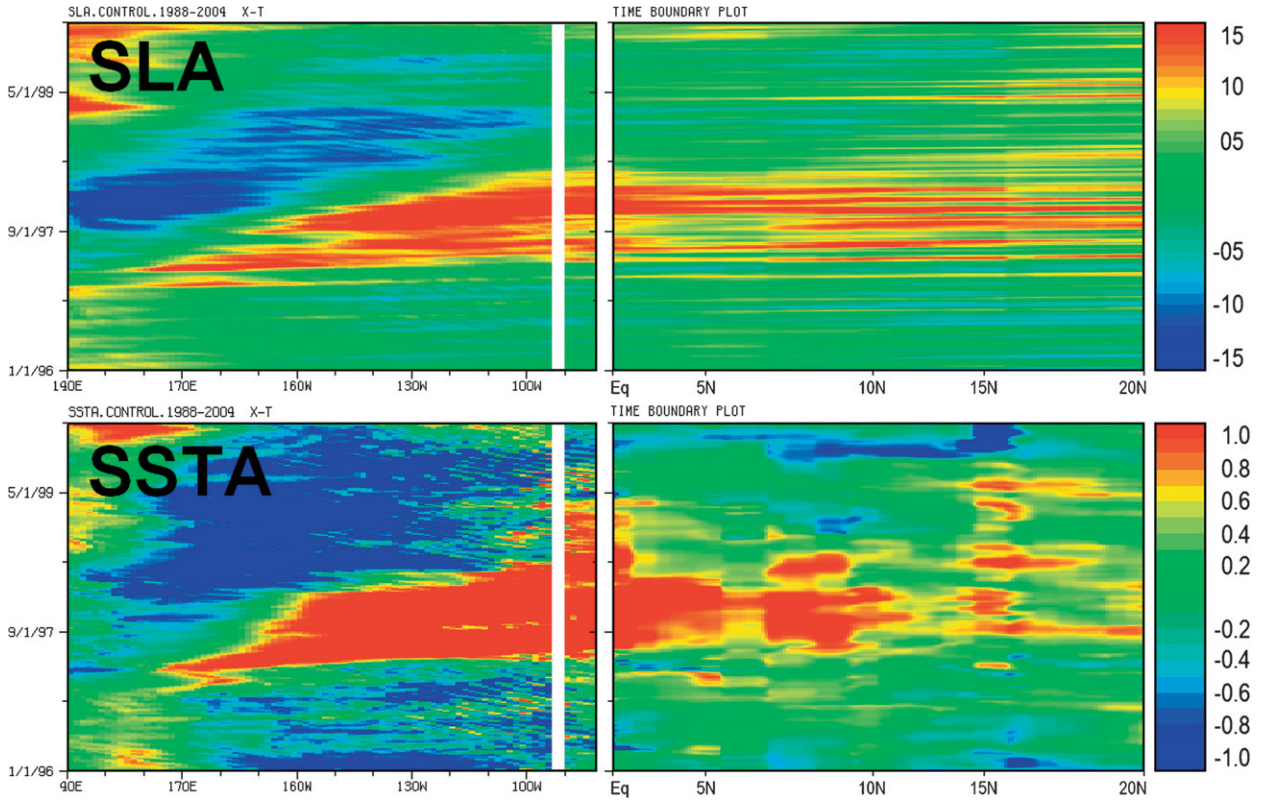

FIG. 13. (top) Equatorial Hovmoeller diagram of SLA (cm) from 140°E to 80°W connected to a boundary Hovmoeller diagram of SLA along the Americas from the equator to 20°N and from the Control experiment between January 1996 and August 1999. (bottom) As in (top), but for SSTA (°C).

the Clim–solar experiment. In this case, one can still discern some of the SSTA signal, which is due to Kelvin waves propagating along the coast, beyond which SST anomalies are very weak until the Gulf of Tehuantepec. The implication is that surface shortwave radiation is responsible for some of the coastal SSTA signal that may otherwise appear to be due to coastal KWs, and is responsible for most of the coastal SSTA signal within the latitude band of the EPWP, which could also have been incorrectly ascribed to an extension of the KW signal originating at the equatorial coast.

To focus on the strong 1997/98 El Niño event, shown in Figs. 13–15 are equatorial Hovmoeller diagrams connected to boundary Hovmoeller diagrams of SLA and SSTA restricted to the period January 1996–August 1999, for experiments Control, Clim–winds, and Clim–solar. This arrangement allows one to seamlessly follow the eastward propagation of equatorial KWs (in terms of SLA) and corresponding SSTA signals across the width of the basin, and subsequent propagation of coastal KWs up the coast of Central America and Mexico. In the Control experiment (Fig. 13), a series of strong equatorially forced coastal KWs are evident. In terms of SSTA, the maximum SSTA along the equator is 3.4°C, along with relatively strong coastal SST anomalies. Other than the anomalies at the Isthmus of Tehuantepec (~15°N), it cannot be determined from Fig. 13 how much of the coastal SSTA signal is actually forced by the propagating KWs. Certainly the analyses thus far would suggest other processes such as surface shortwave radiation could be important even along the coast.

Shown in Fig. 14 is the same depiction as in Fig. 13 but for the Clim–winds experiment. Recall that the Clim–winds experiment does not include interannual wind stress forcing, but does include interannual shortwave forcing. Thus, any SST anomalies along the equator or coast can only be attributable to surface shortwave radiation. Not surprisingly, there are no equatorial or coastal KWs present in the Clim–winds experiment. Also not surprisingly, where there would otherwise be a positive SSTA propagating along the equator during 1997/98, there is instead a negative SSTA. This is because the shortwave forcing is trying to damp a positive SST anomaly that does not exist in this experiment. However, what is notable and confirms the notion that shortwave radiation is important east of the Galápagos

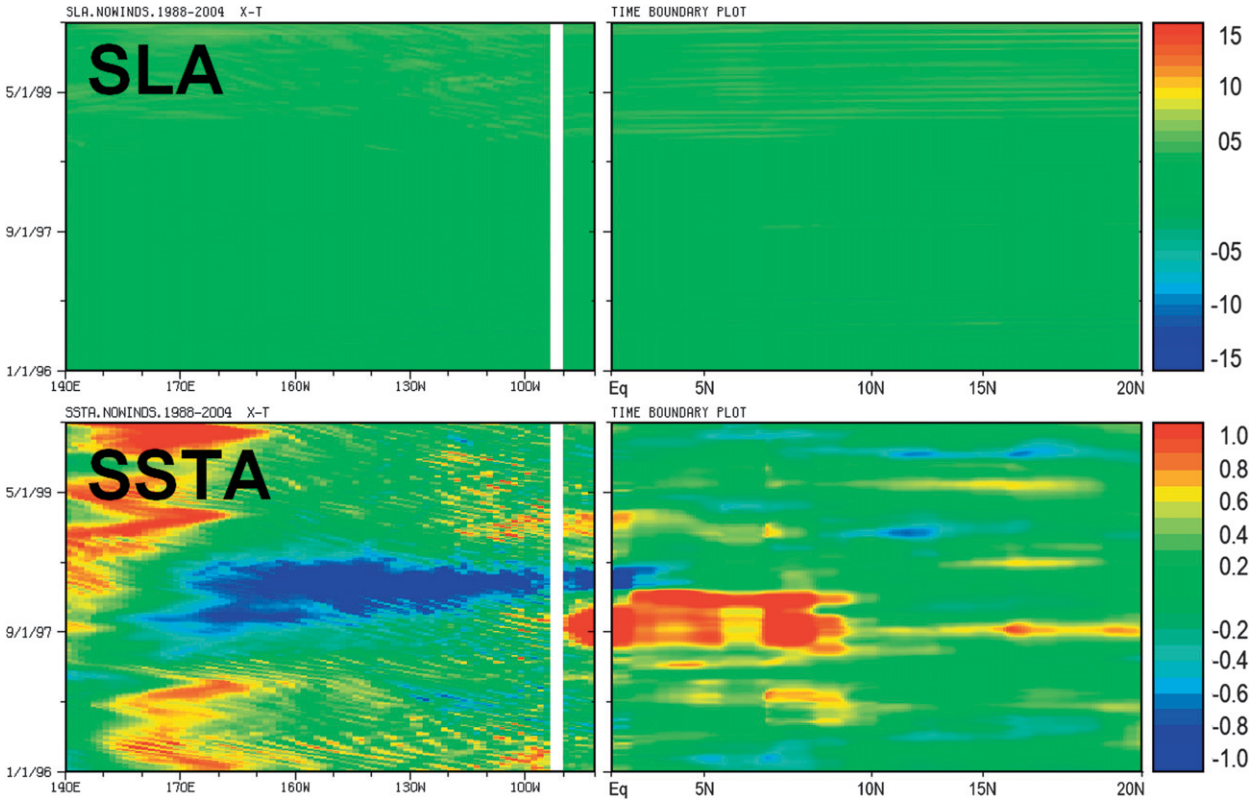

FIG. 14. As in Fig. 13, but for Clim–winds.

Islands and in the EPWP is the positive equatorial SST anomalies east of the Galápagos and coastal anomalies extending well into the EPWP.

We now compare the Control Hovmoeller depiction with that for Clim–solar (Fig. 15). The equatorial and coastal SLA Hovmoeller diagrams for Clim–solar are nearly identical to those of Control; the equatorial and equatorially forced coastal KWs only depend on the wind forcing, which is the same in the two experiments. In terms of SST, the equatorial anomaly is larger in Clim–solar than in Control (4.9° versus 3.4°C) because the shortwave forcing is not present to damp the SST anomaly. Along the coast, comparable (to Control) SST anomalies are present only as far north as about 6°N, while the SST anomalies northward (into the EPWP) of 6°N are much reduced, suggesting that the shortwave forcing is necessary to establish a correlation between the equatorial ENSO signal and SSTA in the EPWP, including the coastal areas of the EPWP, where equatorially forced coastal KWs are prevalent. It is not clear whether the reduced, albeit positive, SST anomalies centered around 10°N are due to KWs or a southward extension of the Tehuantepec gap winds. Given the apparent phase lagging, it would appear to be due to KWs. This, however, may be an exaggerated effect because the amplitude of the ENSO event itself is higher because of the lack of the damping effect of shortwave radiation. As strong as the 1997/98 event was, and regardless of how freely the KWs propagate northward along the eastern boundary in terms of SLA, Fig. 15 confirms that the northern reach of KWs, in terms of continuous SSTA response, is about 6°N, which is effectively the southern limit of the EPWP. This is highly consistent with Kessler (2006, his Fig. 12), although it was interpreted differently. This latitude of 6°N is also consistent with the apparent separation in SLA variability (Fig. 10) and the density gradient (Fig. 11d), although the exact location of the separation between the equatorial and warm pool region varies by a few degrees of latitude depending on which parameter is being considered.

Finally, a brief discussion of the *e*-folding decay scale of coastal KWs is necessary, since that ultimately determines the potential for KWs to impact the SST field in the interior of the EPWP (i.e., away from the coast). The amplitude of a KW decays exponentially away from the coast, with an *e*-folding decay distance given by c/f, or the Rossby radius of deformation, where c is the KW phase speed and f is the magnitude of the Coriolis parameter. Coastal KWs along the Pacific coast of Central America are thought to travel at $c = 2$–3 m s^{-1} (Meyers et al. 1998), and the value of f at 11.5°N (the mean

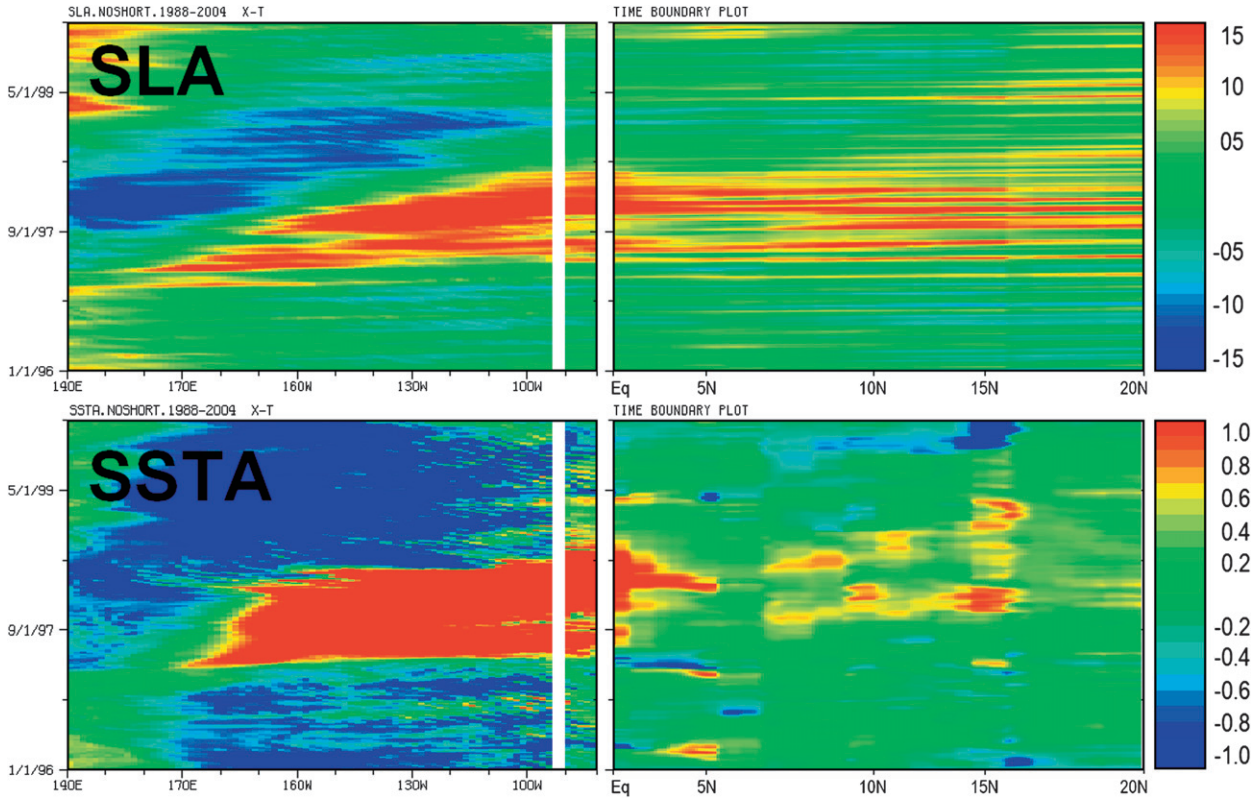

FIG. 15. As in Fig. 13, but for Clim–solar.

latitude of the EPWP as defined in Fig. 1) is 2.9 10^{-5} s^{-1}, resulting in an *e*-folding decay scale for coastal KWs propagating through the EPWP of 69–103 km from the coast, or an order of 1° of latitude or longitude from the coast. Therefore, even if coastal KWs were able to bypass the physics described above which prevents them from strongly impacting coastal SSTs north of ~6°N, their effect would be locally confined to within ~100 km of the coast, whereas the largest SST anomalies are observed and simulated well offshore in the interior of the EPWP.

4. Summary and discussion

The objective of this paper was to identify the physical mechanisms governing the interannual variability of SST in the EPWP. Analysis of SST from satellite observations and a forced ocean model clearly indicated that SST in the EPWP is closely tied to ENSO. Given the close proximity of the EPWP to the equatorial Pacific Ocean, the center of the ENSO surface anomalies, this was not surprising. What was surprising was that the ENSO signal is largely communicated from the equatorial Pacific Ocean to the EPWP not through a direct ocean pathway, but through an atmospheric link. ENSO is therefore effectively a ''remote'' driver of the EPWP.

The mechanism is simple; upward vertical motion in the atmosphere, which results in cloud cover, follows warm water in the tropics. Cloud cover reduces solar heating of the surface, while clear skies pass solar radiation and heat the surface. The east Pacific warm pool is therefore typically a cloudy and rainy region. However, when the equatorial Pacific Ocean is anomalously warm (such as during an El Niño event), cloud cover usually anchored over the western tropical Pacific Ocean and the EPWP is instead situated over the eastern equatorial Pacific Ocean. When such an event occurs, massive anomalous upward vertical motion also occurs over the eastern equatorial Pacific Ocean with compensating descent over the EPWP. Thus, anomalously warm SST in the eastern equatorial Pacific Ocean forces anomalously warm SST in the EPWP using the atmospheric meridional–vertical circulation cell as a link.

While the proposed mechanism for communicating the ENSO signal from the equatorial Pacific Ocean to the EPWP is plausible, it does not by itself prove that ocean transport is unimportant. However, analysis of the ocean mixed layer heat budget and poleward heat transport, including coastal Kelvin waves, suggests that is the case. Also, it is highly consistent with the conspicuous lack of poleward heat transport convergence

between the equatorial Pacific and the northern tropics, while to the south of the equator, poleward heat transports are large (Meinen 2005). Kessler (2006) mentions that many previous studies have identified examples of ocean responses as far north as Alaska to equatorially forced coastal Kelvin waves associated with ENSO. It was shown here that Kelvin waves propagate quite freely along the Pacific coast of the Americas, yet there is very little SSTA response to such waves beyond 6°N. Our model results suggest the range of latitudes corresponding to the EPWP are not strongly subject to this influence. Rather, the results described herein strongly suggest that the EPWP is controlled by ENSO through its effect on the distribution of shortwave radiation.

It is also worthwhile to point out that the mechanism identified in this paper for the interannual variability of SST in the EPWP is not necessarily limited to the domain of the EPWP. The correlation between SSTA along the latitude band of the EPWP and that in the Niño-3 region remains high out to approximately 150°W (30°–40° west of the EPWP according to our definition). While the strongest compensating vertical motion response is found directly over the EPWP, the omega anomalies also extend several tens of degrees longitude west of the EPWP. Further examination of mixed layer heat budget variability at similar off-equatorial locations west of the EPWP suggests that this mechanism likely holds to approximately 150°W, or for the eastern tropical Pacific in general.

One potential uncertainty which could not have been addressed using the approach described in this paper is the role of cloud cover in modulating net longwave radiation. In the OGCM experiments presented herein, the shortwave forcing implicitly includes the effect of interannual cloud cover, while net longwave radiation was computed interactively by the modeled SSTs and atmospheric mixed layer properties, and climatological cloud cover. Thus, one area of future research would be to quantify the contribution of the feedback between SST and longwave radiation via cloud cover.

Since the EPWP is driven by ENSO primarily through an atmospheric link, and given that Central America and southern Mexico are directly adjacent to the EPWP, the processes discussed in this study are relevant to the interannual variability of rainfall in that region. ENSO tends to peak in boreal winter, while the seasonal rainfall in Central America is in boreal summer. During a developing and mature ENSO event, which is when the mechanism described in this study would be in effect, the EPWP could not likely have an impact on rainfall even though that is when the SST anomaly is greatest. However, the EPWP retains the ENSO-driven SST anomaly for several months following the peak event, which has important implications for the variability and predictability of rainfall over Central America and southern Mexico (Karnauskas and Busalacchi 2009).

Acknowledgments. The authors wish to thank Drs. Ernesto Hugo Berbery, Wayne Higgins, Sumant Nigam, and Raghu Murtugudde for guidance throughout the work leading to this manuscript, Mr. Eric Hackert for technical assistance with the ocean model, and two anonymous reviewers for helpful suggestions to improve the manuscript. This research was supported by the National Oceanic and Atmospheric Administration (NOAA) Pan American Climate Studies (PACS) program through Grant NA17EC1483.

REFERENCES

Atlas, R., R. N. Hoffman, S. C. Bloom, J. C. Jusem, and J. Ardizzone, 1996: A multiyear global surface wind velocity dataset using SSM/I wind observations. *Bull. Amer. Meteor. Soc.,* **77,** 869–882.

Bourassa, M. A., D. G. Vincent, and W. L. Wood, 1999: A flux parameterization including the effects of capillary waves and sea state. *J. Atmos. Sci.,* **56,** 1123–1139.

Carton, J. A., G. Chepurin, X. Cao, and B. S. Giese, 2000: A Sample Ocean Data Assimilation analysis of the global upper ocean 1950–95. Part I: Methodology. *J. Phys. Oceanogr.,* **30,** 294–309.

Chen, D., L. M. Rothstein, and A. J. Busalacchi, 1994: A hybrid vertical mixing scheme and its application to tropical ocean models. *J. Phys. Oceanogr.,* **24,** 2156–2179.

Collier, J. C., K. P. Bowman, and G. R. North, 2004: A comparison of tropical precipitation simulated by the community climate model with that measured by the Tropical Rainfall Measuring Mission satellite. *J. Climate,* **17,** 3319–3333.

Enfield, D. B., and S.-K. Lee, 2005: The heat balance of the Western Hemisphere warm pool. *J. Climate,* **18,** 2662–2681.

——, ——, and C. Wang, 2006: How are large Western Hemisphere warm pools formed? *Prog. Oceanogr.,* **70,** 346–365.

Fiedler, P. C., 2002: The annual cycle and biological effects of the Costa Rica Dome. *Deep-Sea Res.,* **49,** 321–338.

Fu, L.-L., E. J. Christensen, C. A. Yamarone Jr., M. Lefebvre, Y. Ménard, M. Dorrer, and P. Escudier, 1994: TOPEX/Poseidon mission overview. *J. Geophys. Res.,* **99** (C12), 24 369–24 382.

Gent, P. R., and M. A. Cane, 1989: A reduced gravity, primitive equation model of the upper equatorial ocean. *J. Comput. Phys.,* **81,** 444–480.

Kalnay, E., and Coauthors, 1996: The NCEP/NCAR 40-Year Reanalysis Project. *Bull. Amer. Meteor. Soc.,* **77,** 437–471.

Karnauskas, K. B., 2007: Interannual variability of sea surface temperature in the eastern tropical Pacific Ocean and Central American rainfall. Ph.D. thesis, University of Maryland, 301 pp. [Available online at http://www.lib.umd.edu/drum/bitstream/1903/7706/1/umi-umd-4983.pdf.]

——, and A. J. Busalacchi, 2009: The role of SST in the east Pacific warm pool in the interannual variability of Central American rainfall. *J. Climate,* in press.

——, ——, and R. Murtugudde, 2008: Low-frequency variability and remote forcing of gap winds over the east Pacific warm pool. *J. Climate,* **21,** 4901–4918.

Kessler, W. S., 2006: The circulation of the eastern tropical Pacific: A review. *Prog. Oceanogr.,* **69,** 181–217.

——, L. M. Rothstein, and D. Chen, 1998: The annual cycle of SST in the eastern tropical Pacific, diagnosed in an ocean GCM. *J. Climate,* **11,** 777–799.

Kiehl, J., J. Hack, G. Bonan, B. Boville, B. Briegleb, D. Williamson, and P. Rasch, 1996: Description of the NCAR Community Climate Model (CCM3). NCAR Tech. Rep. NCAR/TN–420+STR, 152 pp.

Kraus, E. B., and S. J. Turner, 1967: A one-dimensional model of the seasonal thermocline. Part II. *Tellus,* **19,** 98–105.

Kummerow, C., and Coauthors, 2000: The status of the Tropical Rainfall Measuring Mission (TRMM) after two years in orbit. *J. Appl. Meteor.,* **39,** 1965–1982.

Lee, S.-K., D. B. Enfield, and C. Wang, 2005: Ocean general circulation model sensitivity experiments on the annual cycle of Western Hemisphere warm pool. *J. Geophys. Res.,* **110,** C09004, doi:10.1029/2004JC002640.

——, ——, and ——, 2007: What drives the seasonal onset and decay of the Western Hemisphere warm pool? *J. Climate,* **20,** 2133–2146.

Levitus, S., and T. Boyer, 1994: *Temperature*. Vol. 4, *World Ocean Atlas,* NOAA Atlas NESDIS 4, 117 pp.

Liebmann, B., and C. A. Smith, 1996: Description of a complete (interpolated) outgoing longwave radiation dataset. *Bull. Amer. Meteor. Soc.,* **77,** 1275–1277.

Maloney, E. D., and J. T. Kiehl, 2002: Intraseasonal eastern Pacific precipitation and SST variations in a GCM coupled to a slab ocean model. *J. Climate,* **15,** 2989–3007.

——, and S. K. Esbensen, 2003: The amplification of east Pacific Madden–Julian oscillation convection and wind anomalies during June–November. *J. Climate,* **16,** 3482–3497.

——, and ——, 2005: A modeling study of summertime east Pacific wind-induced ocean–atmosphere exchange in the intraseasonal oscillation. *J. Climate,* **18,** 568–584.

McPhaden, M. J., and Coauthors, 1998: The Tropical Ocean Global Atmosphere observing system: A decade of progress. *J. Geophys. Res.,* **103,** 14 169–14 240.

Meinen, C. S., 2005: Meridional extent and interannual variability of the Pacific Ocean tropical–subtropical warm water exchange. *J. Phys. Oceanogr.,* **35,** 323–335.

Meyers, S. D., A. Melsom, G. T. Mitchum, and J. J. O'Brien, 1998: Detection of the fast Kelvin wave teleconnection due to El Niño-Southern Oscillation. *J. Geophys. Res.,* **103,** 27 655–27 663.

Murtugudde, R., R. Seager, and A. Busalacchi, 1996: Simulation of the tropical oceans with an ocean GCM coupled to an atmospheric mixed-layer model. *J. Climate,* **9,** 1795–1815.

Pinker, R. T., and I. Laszlo, 1992: Modeling of surface solar irradiance for satellite applications on a global scale. *J. Appl. Meteor.,* **31,** 194–211.

Price, J. F., R. A. Weller, and R. Pinkel, 1986: Diurnal cycling: Observations and models of the upper ocean response to diurnal heating, cooling, and wind mixing. *J. Geophys. Res.,* **91,** 8411–8427.

Reynolds, R. W., N. A. Rayner, T. M. Smith, D. C. Stokes, and W. Wang, 2002: An improved in situ and satellite SST analysis for climate. *J. Climate,* **15,** 1609–1625.

Sadler, J. C., 1964: Tropical cyclones of the eastern North Pacific as revealed by TIROS observations. *J. Appl. Meteor.,* **3,** 347–366.

Seager, R., M. B. Blumenthal, and Y. Kushnir, 1995: An advective atmospheric mixed layer model for ocean modeling purposes: Global simulation of surface heat fluxes. *J. Climate,* **8,** 1951–1964.

Sun, D.-Z., 2000: The heat sources and sinks of the 1986–87 El Niño. *J. Climate,* **13,** 3533–3550.

Wang, C., and D. B. Enfield, 2001: The tropical Western Hemisphere warm pool. *Geophys. Res. Lett.,* **28,** 1635–1638.

——, and ——, 2003: A further study of the tropical Western Hemisphere warm pool. *J. Climate,* **16,** 1476–1493.

——, ——, S.-K. Lee, and C. W. Landsea, 2006: Influences of the Atlantic warm pool on Western Hemisphere summer rainfall and Atlantic hurricanes. *J. Climate,* **19,** 3011–3028.

Webster, P. J., and R. Lukas, 1992: TOGA–COARE: The Coupled Ocean–Atmosphere Response Experiment. *Bull. Amer. Meteor. Soc.,* **73,** 1377–1416.

Wyrtki, K., 1964a: Upwelling in the Costa Rica Dome. *Fish. Bull.,* **63,** 355–372.

——, 1964b: Surface currents of the eastern tropical Pacific Ocean. *Bull. Inter-Amer. Trop. Tuna Comm.,* **9,** 270–304.

Xie, S.-P., H. Xu, W. S. Kessler, and M. Nonaka, 2005: Air–sea interaction over the eastern Pacific warm pool: Gap winds, thermocline dome, and atmospheric convection. *J. Climate,* **18,** 5–20.

Zhang, C., 1993: Large-scale variability of atmospheric deep convection in relation to sea surface temperature in the tropics. *J. Climate,* **6,** 1898–1913.